Arab J Sci Eng (2016) 41:281–300
DOI 10.1007/s13369-015-1806-7

RESEARCH ARTICLE - EARTH SCIENCES

Geological and Petrophysical Characterization of the Lower Senonian Matulla Formation in Southern and Central Gulf of Suez, Egypt

Mohamed S. El Sharawy[1] · **Bassem S. Nabawy**[1]

Received: 9 January 2015 / Accepted: 23 July 2015 / Published online: 6 August 2015

Abstract The Lower Senonian Matulla Formation is well developed in the southern and central Gulf of Suez. It can be subdivided into three depositional units (M1–M3). An obvious unconformity separated the middle unit (M2) from the upper unit (M3). The three units are corresponding to a second-order depositional sequence. This sequence consists of two systems tracts; the lower lowstand systems tract consists of slope fan, followed by a prograding complex. An erosion surface separated the lower from the upper transgressive systems tract. The Matulla Formation is mostly composed of sandstones and pelagic sediment intercalations. Such intercalations show obvious facies change throughout the study area, causing further subdivision of the Matulla Formation into seven rock types (RT1–RT7). The petrophysical reservoir evaluation has been achieved via determination of the effective porosity, permeability, shale content, water saturation and net-pay thickness from the environmentally corrected well log data. It indicates that the Matulla Formation can be considered as a good reservoir quality especially in its lower unit and sometimes in its middle unit as well. The available core data indicate a lithological heterogeneity of the studied Matulla Formation. Lithologically, it can be subdivided into four petrophysical and lithological facies; namely, they are sandstones, ferruginous sandstones, argillaceous sandstones and limestones. The best petrophysical properties were assigned for the ferruginous sandstones with good to excellent porosity, very good to excellent permeability, and poor to fair flow zone indicator.

✉ Mohamed S. El Sharawy
sharawy2001@hotmail.com

[1] Department of Geophysical Sciences, National Research Centre, Cairo, Egypt

Keywords Matulla Formation · Gulf of Suez · Porosity · Permeability · Reservoir characterization · Flow units

1 Introduction

The Late Cretaceous deposits are well developed throughout Egypt. This is due to a transgression phase associated with the subsidence caused by the neo-Tethyan rift event that took place across the northern margin of Africa, resulting in a period of dominantly marine deposits in the Gulf of Suez [1]. The Late Cretaceous Nezzazat Group was introduced by Steen and Helmy [2] to represent the Cenomanian, Turonian and clastic sediments of the Lower Senonian. The Nezzazat Group has been divided into four formations namely, from base to top, the Raha Formation, the Abu Qada Formation, the Wata Formation and the Matulla Formation. The Lower Senonian Matulla Formation is the most important clastic sequence in the Nezzazat Group because it provides the highest net reservoir thickness and the highest net/gross ratio. Moreover, it is occurred everywhere throughout the Gulf of Suez. The Nezzazat Group was studied by several authors, e.g., Hassouba et al. [3], who discussed the depositional environments and the sedimentary aspects of the Nezzazat Group in October oil field (Central Gulf of Suez). Marttila and El Bahr [4] studied the Nezzazat Group in different fields throughout the Gulf of Suez. They concluded that the rock complexity of the Nezzazat Group has insignificant impact on the ability to calculate the reservoir parameters using well logs. However, other factors such as sand continuity, recovery factor and drive mechanism have much larger impact on the oil-in-place than the mineralogical complexity. El Bahr et al. [5] studied the effect of glauconite in October and Razzak fields (Central Gulf of Suez and Western Desert, respectively) on the petrophysical reservoir characteristics

of the Nezzazat Group. They concluded that 20 % of glauconite content in rocks gives 4 % shift in porosity. Recently, El-Azabi and El-Araby [6] divided the Matulla Formation into three third-order depositional sequences deposited during the transgressive and highstand systems tracts. The main purpose of the present study is to evaluate the geological, petrophysical and reservoir properties of the Matulla Formation in some locations (Fig. 1) in the central and southern Gulf of Suez, using well logs and seismic data as well as routine core analysis.

The well log data, routine core analyses as well as the oil and water saturation measured from cores of some wells were used to evaluate the petrophysical properties and oil potentiality of the Matulla Formation and to conduct a reservoir zonation and discrimination of the conductive zones in this formation. The reservoir quality and flow zone discrimination was applied using the technique of Amaefule et al. [7], which allows a more precise reservoir discrimination using permeability and porosity data.

The reservoir quality index 'RQI' of Amaefule et al. [7] can be used to characterize the different flow zones of a reservoir to provide a good relationship between petrophysical properties from the core plug scale to the well bore scale. It was successfully applied by many authors to determine the reservoir quality, e.g., [8–10].

2 Measuring and Processing Techniques

The well log data for eight wells distributed in the central trough of the southern Gulf of Suez as well as the southern part of the Central Gulf of Suez were used in the present study (Fig. 1). The selected wells are belonging to eight fields, namely they are, from northwest to southeast, Belayim Marine, Amal, GS365, GS373, SB 374, Sidki, East Zeit and Hilal. Except for Belayim Marine and Amal fields to the north of the studied area, the Nezzazat Group is represented in these fields by the Matulla Formation with absence of the lower three formations of Nazzazat Group in most of the studied wells (Wata, Abu Qada and Raha Formations) due to uplifting and erosion which are related to the Turonian uplifting [11,12].

The well log data include gamma ray, spectral gamma ray, neutron, density, sonic, resistivity (shallow and deep), Pe curve and dipmeter.

Definition of the rock types of the Matulla Formation was carried out using the IP software program, in which we used gamma ray, density, neutron, sonic and resistivity logs as inputs and the rock types as outputs. The cluster randomness plot method was used to provide the best results by which we can determine the most optimum number of the rock types.

For more accurate lithologically and petrophysically evaluation of the Matulla Formation, a mineral solver model using the IP program was applied to detect possible mineral composition, total and effective porosity, shale volume, fluid saturation and net-pay thickness. For shaly sand, several models were proposed to solve the problem. For the studied formation; the best results were obtained by using the modified Indonesian model, which has the following form:

$$\frac{1}{\sqrt{R_t}} = \left(\frac{(V_{\mathrm{sh}})^{\frac{(1-V_{\mathrm{sh}})}{2}}}{\sqrt{R_{\mathrm{sh}}}} + \sqrt{\frac{\phi^m}{a R_{\mathrm{w}}}} \right) S_{\mathrm{w}}^{\frac{n}{2}}$$

where:

S_{w} is the water saturation, in fraction,
n is the saturation exponent, dimensionless,
a is the formation factor coefficient, dimensionless,
R_{w} is the formation water resistivity, in ohm m,
R_{t} is the true formation resistivity, in ohm m,
m is the cementation exponent, dimensionless,
Ø is the porosity, in fraction,
V_{sh} is the shale content, in fraction, and
R_{sh} is the resistivity in front of shale, in ohm m.

Plotting the dip azimuth and magnitude of the studied beds versus depth as well as the clustering direction and magnitude enabled revealing the geologic setting and structural elements prevailed in the studied wells GS2 and SDK7 (GS373 and Sidki oil fields, respectively).

In addition to processing the environmentally corrected well log data, the routine core analyses have been conducted for 177 cored plugs through the Matulla Formation in two oil wells, 'BM-85' is representative for the Belayim Marine oil field in the central Gulf, and the other 'H-A4' is located in Hilal oil field in the southern Gulf of Suez (Fig. 1).This interval corresponds to the upper part of the middle unit (M2) and the lower part of the upper unit (M3) of Matulla in Hilal oil field and to the lower unit (M1) of the Matulla Formation in Belayim Marine field.

The routine core analyses include measurement of bulk and grain densities, helium porosity, vertical and horizontal gas permeability as well as water and oil saturation (Table 1). The analyzed interval consists of sandstones with some intercalations of shales. The limestone facies was assigned to the north in Belayim Marine oil field.

3 Geologic and Structural Setting

Structural setting and tectonic evolution of the Gulf of Suez were studied by numerous authors [1,13–22]. Structurally, the Gulf of Suez was divided into three provinces separated by two accommodation zones. The Southern Gulf of Suez

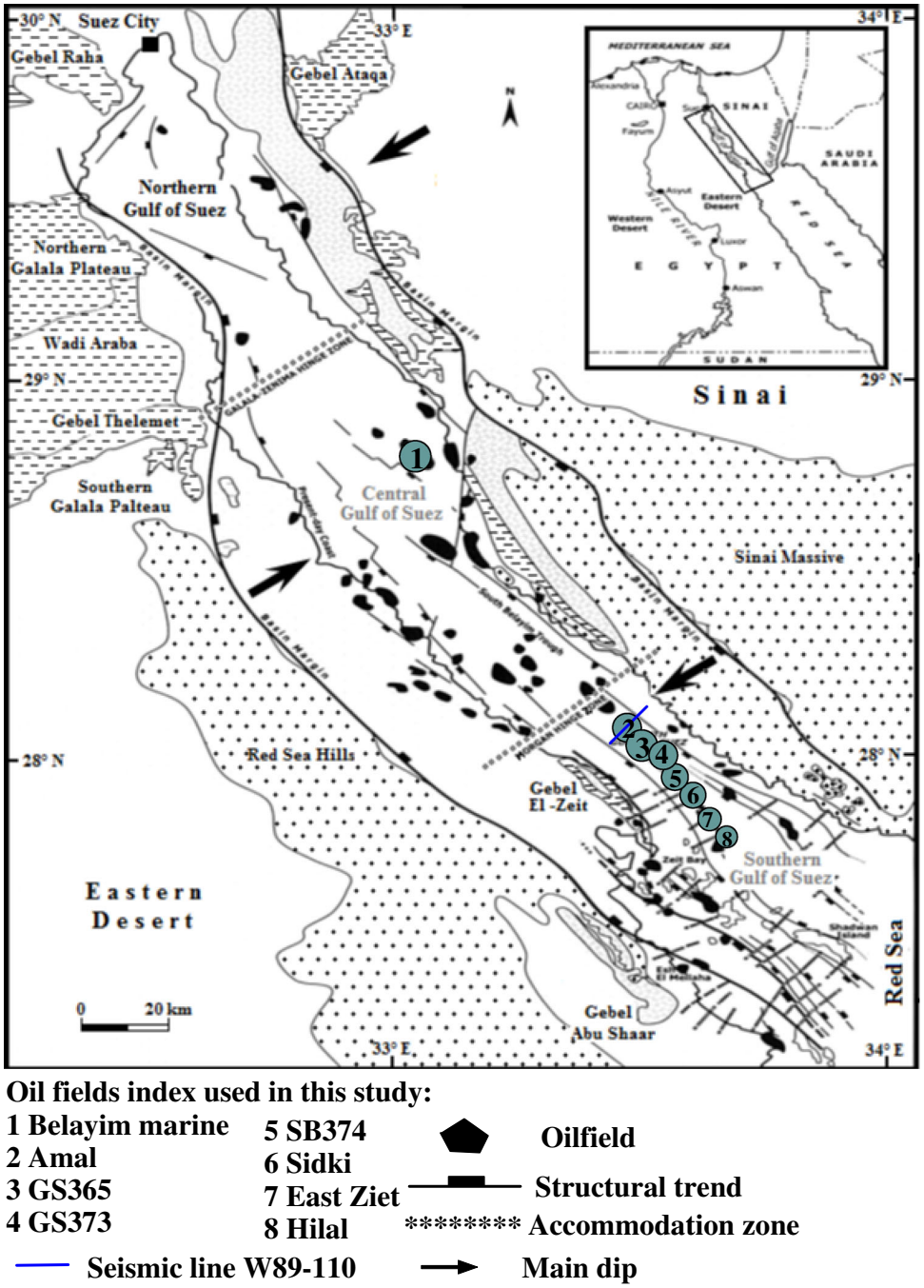

Fig. 1 Location map of the study area showing the distribution of studied wells and the main structural settings in the Southern Gulf of Suez, modified after [22]

was further subdivided into several structural trends, in which the central trough is called the "B-Trend" (Fig. 1). This prolific trend is characterized by development of salt diapirs and production of hydrocarbon from pre- and syn-rift strata. It is also characterized by the fault–tilt blocks, which controlled mainly by two sets of fault trends.

Due to the Oligocene-Early Miocene rifting, the Gulf of Suez stratigraphic succession is usually divided into pre- and syn-rift strata. The prerift succession includes two lithofacies. The lower lithofacies includes the fluvial braided system to eolian environment Nubia sandstone, which considered as one of the main reservoirs in the Gulf area. This Nubia interval is composed of consolidated sandstone ranged in age from Cambrian to Lower Cretaceous and increased in thickness from southern to northern Gulf of Suez. The second lithofacies includes the sediments of the Late Cretaceous—Eocene transgression phase, which resulted in intercalations of sandstone, shale and carbonate. The thickness of the prerift strata ranges from about 500 ft to more than 1000 ft according to the thickness of the Nubia sandstone.

The syn-rift stratigraphic succession consists of intercalations of sandstone, shale, carbonate and evaporite. The noticeable vertical and lateral facies changes depend on tectonic activity (subsidence or uplift), fall or rise of sea level, sediments supply, geographic position of the depositional basin (peripheral or depocenter) and temperature. Combination of such factors controlled the facies and thickness of the syn-rift deposits. About 10,000 ft thick or more can be encountered in the syn-rift succession especially in the depocenters such as the "B-Trend." The syn-rift sediments provide reservoir, source and seal rocks.

The development of salt diapirs can be viewed as the main structural feature that characterized the central trough of the southern Gulf of Suez. Such salt diapirs provided the ultimate

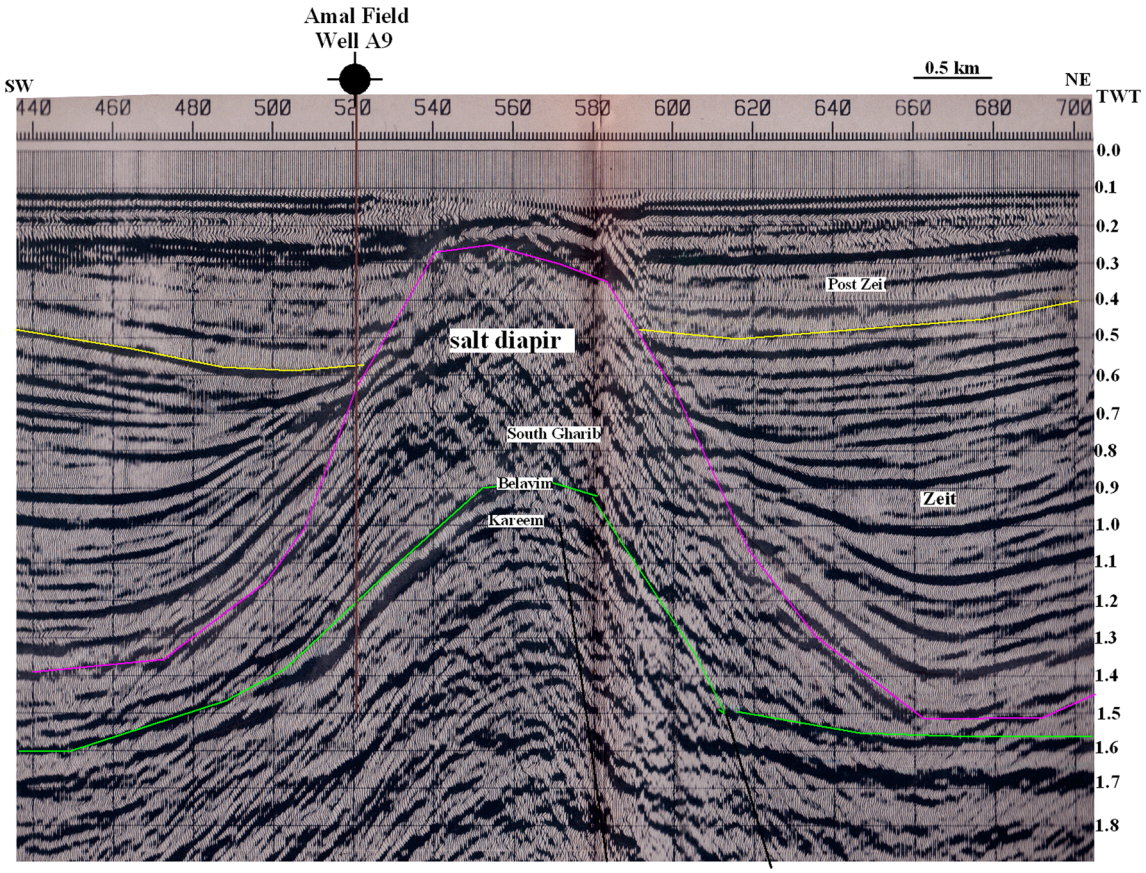

Fig. 2 Seismic line W89–110 interpretation showing the size of salt diapir in the northern part of the B-Trend (for location, see Fig. 1)

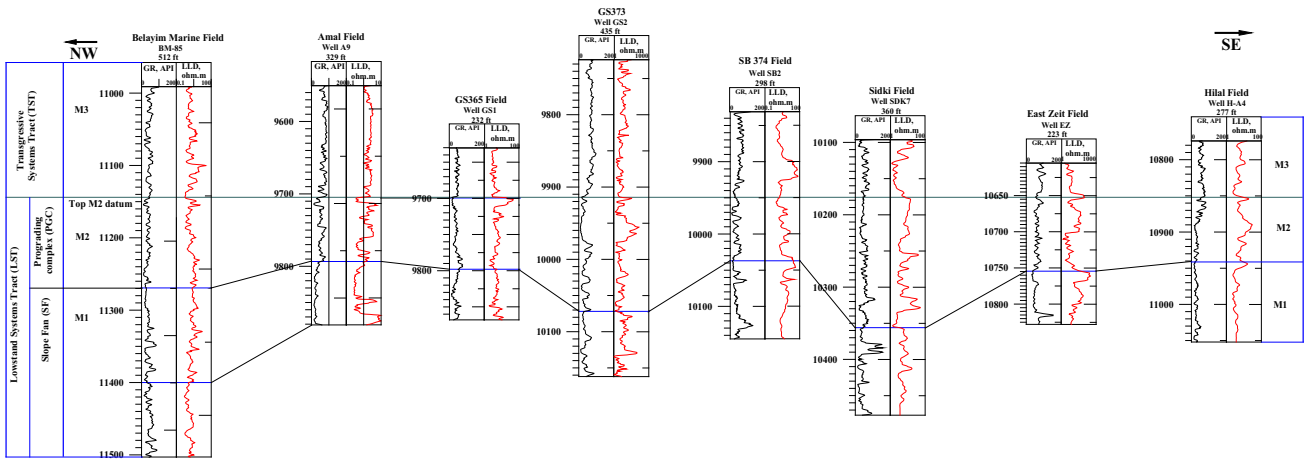

Fig. 3 Well-to-well correlation showing the interpreted systems tracts and division of the Matulla Formation into three units; M1, M2 and M3. For well locations, see Fig. 1

reservoir seal. Depositional environment and structural configuration of the Gulf of Suez during the abandoned stage of the Suez rift evolution gave the chance to precipitate a huge thickness of evaporites. The subsequence loading of the post-Miocene sediments coupled with pressure and temperature led to mobility of the salt. According to Rowan [23] and Warren [24], the movement of the salt in extensional basin, such as the Gulf of Suez, can be triggered by two mechanisms, differential loading and extension. Therefore, the salt has to be triggered by the effect of overburden and the Pliocene extension. As a result of the uniform of overburden, salt diapirs formed toward the central axis of the Gulf of Suez. Toward the Gulf of Suez margins, salt pillows have been formed instead. The size of the salt diapirs is small at the southern part of the study area. Increasing in size is noticed northward and another decreasing is recorded at the most northern part of the B-Trend (Fig. 2).

Two major sets of fault trends can be inferred from the seismic profile interpretation in the B-Trend area [22]. These two trends are NW–SE clysmic trend and the WSW–ENE cross trend. Combinations of these trends resulted in the characteristic zigzag fault pattern of the fault–tilt blocks.

As a prerift sequence, the Matulla Formation is considered as the main secondary reservoir in the Gulf of Suez

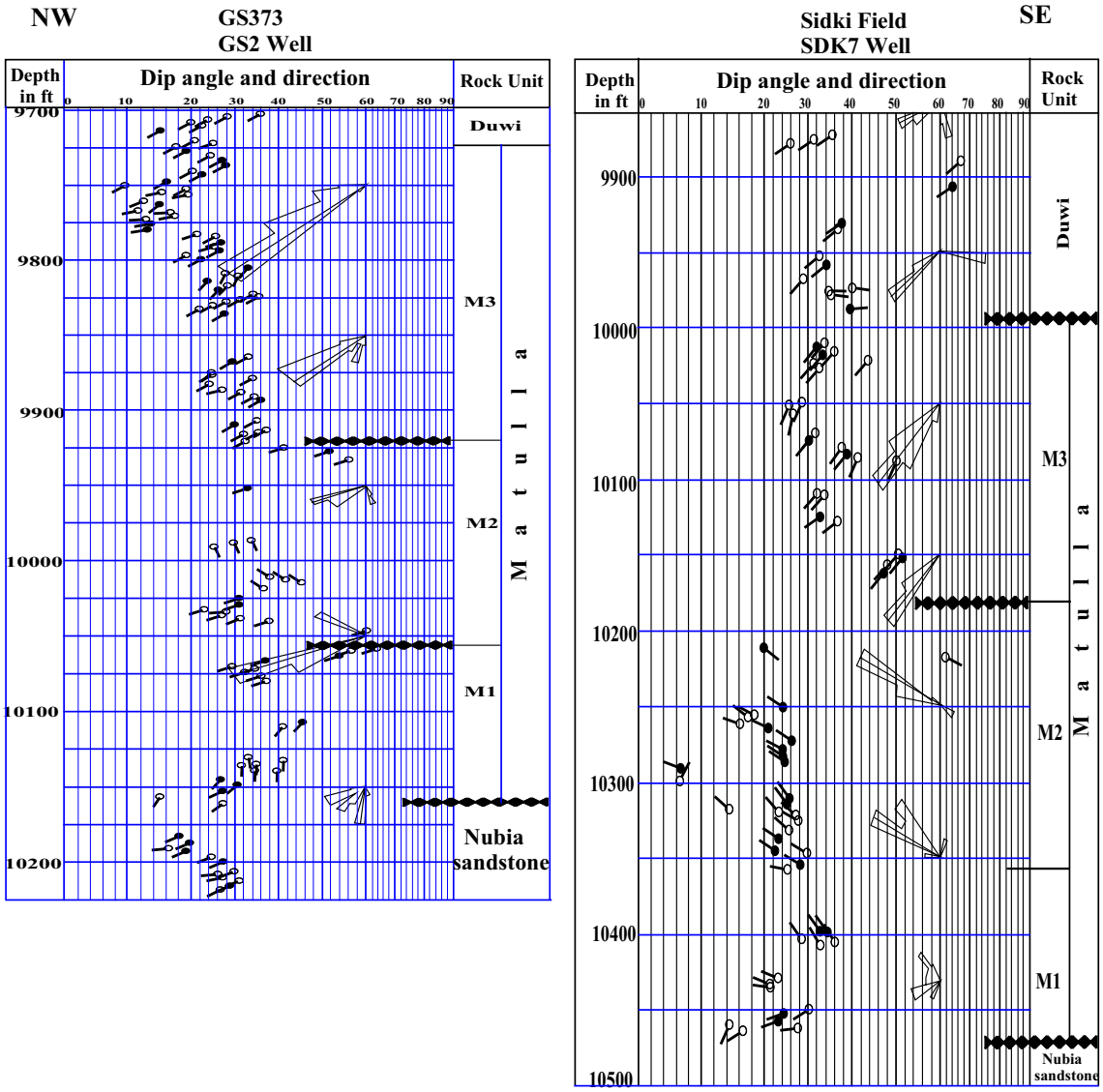

Fig. 4 Dipmeter of GS2 and SDK7 wells illustrated the dip azimuth and magnitude as well as the unconformities between the three Matulla units. Obvious unconformity separated M2 and M3 units was shown in both wells. Possible unconformity could be detected between M1 and M2 units in GS2 well. The overlain and underlain Matulla Formation unconformities can be shown in both wells. Notice the general SW structural trend in the southern Gulf of Suez

province. Oil is produced from many fields, such as Belayim marine, Morgan, October, Hilal, GS365, East Zeit, Amal and Abu Rudeis [25]. The Matulla Formation is often thought to be a reflective of regressive phase compared with the conditions that prevailed throughout the Turonian. The formation generally rests unconformably on the Wata Formation and underlies unconformably the Duwi Formation. The Matulla Formation was usually divided into three units [3,4,26]. According to Hassouba et al. [3], it was deposited in a shallow marginal marine environment. The Matulla Formation consists mainly of sandstone, shale and carbonate intercalations, which contain accessory minerals, such as pyrite and glauconite. The presence of pyrite and glauconite implies deposition in a partially restricted marine environment.

4 Results and Interpretations

4.1 Facies Analysis

From the well log data, the gross thickness of the Matulla Formation ranges from 223 to 512 ft, with an average thickness of 333 ft (Fig. 3). The lithology is mainly a sandstone–shale intercalation. Based on the well-to-well correlation, the Matulla Formation can be divided into three units (Fig. 3); the lower one (M1) consists mainly of sandstone. The sandstone increases with increasing ferruginous content, and the carbonate facies appears northward with decreasing glauconite in the same direction. The middle unit (M2) consists mainly of shales intercalating with sandstones. Glauconite and pyrite tend to decrease northward in this unit. The upper unit (M3) is composed mainly of shales. The shales are composed of mixed-layer clay northward and become mainly ferruginous southward. From the dipmeter processed data, a distinct unconformity separates the middle unit from the upper unit through the different wells (Fig. 4).

Applying the cluster randomness plot, seven facies in the Matulla Formation can be detected. The rock types (labeled RT1 to RT7) are thus ranged from good-quality sandstone to shale (Fig. 5). RT1 (gray) occurs in the M1 and M2 units, and increases in the central part of the studied area. This rock type is sandstone. This rock unit can be considered as a good-quality reservoir. RT2 (green) is a fine-grained glauconitic sandstone. It occurs mainly in the H-A4 and GS1 wells

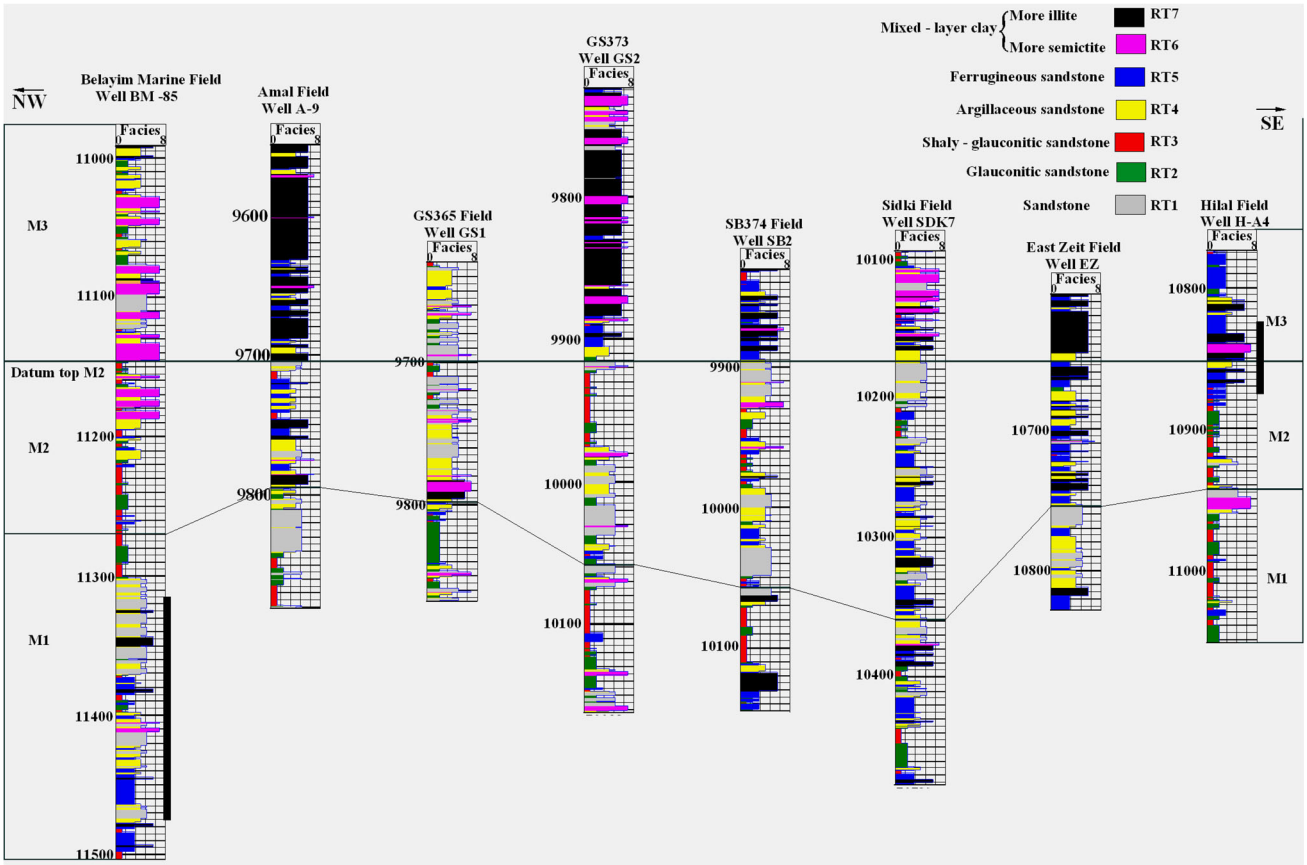

Fig. 5 The distribution of the Matulla Formation seven rock types as interpreted using cluster analysis for rock typing module of IP software program. There is a gradual facies change from north to south as response probably to sea-level fluctuation. *Black bars* represented the cored interval

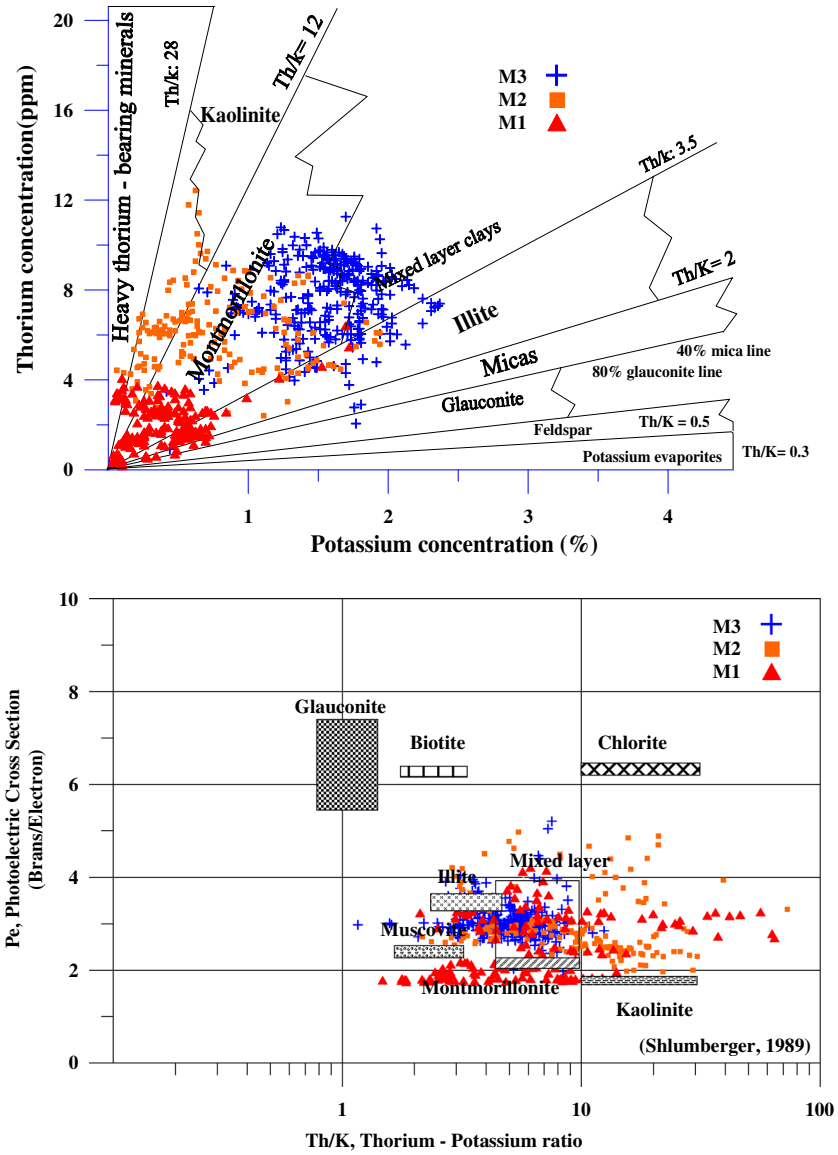

Fig. 6 Identification of clay minerals from thorium, potassium and Pe curve in A19 well (Amal Field). The dominant clay minerals are montmorillonite and illite with low percentage of kaolinite and mica

within the M1 and M2 units. RT3 unit (red) tends to occur in the central and northern parts, mostly within the M1 unit. It is shaly-glauconitic sandstone. This clastic facies shows partial change to a calcareous facies northward in the well Belayim Marine field. RT4 (yellow) occurs in the three units but mostly in the M2 unit. It could be argillaceous sandstone. RT5 (blue) occurs in all the units, but increases southward. It is a ferruginous sandstone. RT6 (purple) occurs mostly in the M3 unit and increases northward. It is a mixed-layer clay, mostly montmorillonite. RT7 (black color) occurs mostly in the M3 unit and increases northward reflecting the direction of transgression. It is a mixed-layer clay, mostly illite.

The core description indicates that the shale is gray to dark gray and hard, with some pyrite content. The sandstone is mostly dark gray, fine to very fine-grained, well cemented and slightly argillaceous to pyritic. The argillaceous sandstone is mostly dark brown, well cemented, very fine, slightly ferruginous, gypsiferous and locally silty. These two clastic facies are dominant in all of the studied wells. The ferruginous sandstone is gray, medium-grained and slightly cemented, while the limestone is grayish brown, well crystallized and impervious.

Presence of spectral gamma ray log and Pe curve in A9 well (Amal field) can be used graphically to determine the type of clays. The crossplots indicate that the clay minerals are mainly illite and montmorillonite with mixed-layer clays and kaolinite (Fig. 6). Traces of mica and glauconite can also be observed. Thorium–uranium ratio 'Th/U' versus thorium–potassium ratio 'Th/K' indicates that kaolinite is restricted to the lower two units (M1 and M2) (Fig. 7). The constraint numbers (2 and 7) were adopted after Adams and Weaver [27].

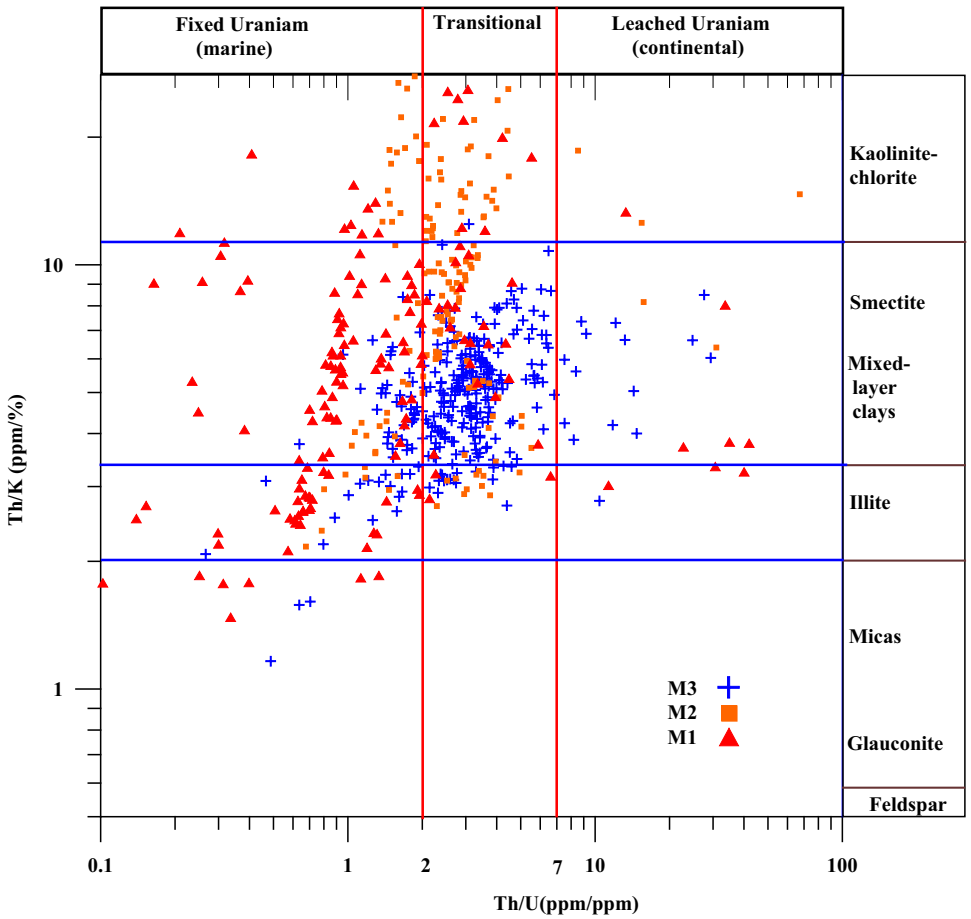

Fig. 7 Thorium–uranium ratio versus thorium–potassium ratio in A9 well (Amal Field) illustrating the depositional environment prevailed during deposition of the Matulla Formation. As noted, M2 unit is restricted mainly in transitional condition, while M1 unit is mainly marine. The constraint numbers (2 and 7) were adopted after Adams and Weaver [30]

4.2 Petrophysical Properties of the Matulla Formation

The average bulk density varies greatly from 2.00 g/cm^3 for the ferruginous sandstones up to 2.48 g/cm^3 for the limestone. The average grain density varies from 2.74 to 2.94 g/cm^3 for the same facies. The relatively high values assigned for the grain density of the Matulla Formation may be attributed to some content of iron oxides and heavy minerals. The average porosity of the studied samples varies from 12.9 % for the limestone up to 26.3 % for the ferruginous sandstone; the minimum value recorded for the limestone is 2.6 % and the maximum value for the ferruginous sandstone is 32.6 % (Table 1). The average measured porosity is ranked as fair to excellent, with ranks of 2–5 [10,27] (Table 2). The measured fluid summation porosity indicates that 'Sw' varies from 35.9 % for the ferruginous sandstone up to 74.4 % for the limestone facies.

Full reservoir description cannot be completed without determination of permeability in which the reservoir permeability is the main contributor to enhancing the reservoir quality and the main key tool for reservoir zonation. However, the accurate determination of permeability is one of the obstacles facing the petrophysicists. According to Ahmed et al. [28], there are three major permeability measurement techniques. These techniques are well logs, such as RFT, NMR and empirical correlations, as well as laboratory core testing and Drill Stem Testing (DST). For the present study, we predicted permeability by using Timur [29] empirical equation and neural network. In the neural network, we used the core data analyses for H-A4 and BM-85 wells to predict permeability. Depth matching and correction logs for the environmental conditions are the basic two steps prior to calculations. Gamma ray, density and sonic logs were used as inputs data and the predicted permeability as output. The results show good matching between the measured and predicted permeability (Fig. 8).

Though the average measured porosity values are accepted to a fair reservoir, the measured average vertical and horizontal core permeability (k_V & k_H) for the studied facies varies greatly between an impervious '0.01 md' and very good '1744 md' with petrophysical ranks of 0–4 (Table 2). The highest average k_V & k_H values are recorded for the ferruginous sandstone facies (754 and 722 md, respectively), while the lowest values were recorded for the limestone facies (0.33 and 0.58 md, respectively).

Table 1 The bulk and grain density (ρ_b, ρ_g), helium porosity ($Ø_{He}$), vertical and horizontal permeability (K_H, K_V), water saturation (S_w), oil saturation (So), reservoir quality index (RQI) and flow zone index (FZI) data for the studied core samples, the Matulla Formation in BM-85 (Belayim Marine) and H-A4 (Hilal) oilfields

Lithology	No.	ρ_b (g/cm^3)	ρ_g (g/cm^3)	$Ø_{He}$ (%)	K_H (md)	K_V (md)	So (%)	Sw (%)	RQI (μm)	FZI (μm)
Sandstones	*79 Plugs*									
	Mean	2.28	2.75	16.6	13.9	12.2	23.4	53.6	0.25	1.52
	Min.	1.91	2.61	2.6	0.20	0.02	0.0	8.0	0.08	0.50
	Max.	2.78	3.29	29.4	67.5	154.6	77.2	87.0	0.54	4.83
Argillaceous sandstones	*35 Plugs*									
	Mean	2.38	2.81	14.5	0.60	0.31	11.2	67.6	0.06	0.50
	Min.	2.09	2.67	2.8	0.07	0.04	0.0	12.7	0.03	0.16
	Max.	2.80	3.23	25.4	2.77	1.35	63.6	95.1	0.11	2.06
Ferruginous sandstones	*45 Plugs*									
	Mean	2.00	2.74	26.3	722	754	35.9	35.9	1.55	4.28
	Min.	1.86	2.64	19.0	276	126	4.9	8.8	1.08	3.13
	Max.	2.12	2.88	32.6	1744	2560	66.7	71.1	2.37	6.21
Limestones	*18 Plugs*									
	Mean	2.48	2.94	12.9	0.58	0.33	1.5	74.4	0.05	0.40
	Min.	2.23	2.71	3.3	0.02	0.01	0.0	39.0	0.02	0.16
	Max.	2.71	3.47	22.9	3.52	0.82	9.7	92.4	0.12	0.92

Table 2 Proposed ranks for the measured porosity, permeability, RQI and FZI

Porosity (%)	Rank	Permeability (md)	Rank	RQI (μm)	Rank	FZI (μm)	Rank
$0 < Ø \leq 5$	0	$0 < K \leq 1$	0	$0.00 < \text{RQI} \leq 0.25$	0	$0.00 < \text{FZI} \leq 1.00$	0 Impervious
$5 < Ø \leq 10$	1	$1 < K \leq 10$	1	$0.25 < \text{RQI} \leq 0.50$	1	$1.00 < \text{FZI} \leq 2.50$	1 Poor
$10 < Ø \leq 15$	2	$10 < K \leq 100$	2	$0.50 < \text{RQI} \leq 1.00$	2	$2.50 < \text{FZI} \leq 5.00$	2 Fair
$15 < Ø \leq 20$	3	$100 < K \leq 1000$	3	$1.00 < \text{RQI} \leq 2.00$	3	$5.00 < \text{FZI} \leq 10.0$	3 Good
$20 < Ø \leq 25$	4	$1000 < K \leq 10000$	4	$2.00 < \text{RQI} \leq 5.00$	4	$10.0 < \text{FZI} \leq 15.0$	4 Very good
$25 < Ø$	5	$10000 < K$	5	$5.00 < \text{RQI}$	5	$15.0 < \text{FZI}$	5 Excellent

The Reservoir Potentiality Index 'RPI' used to characterize and discriminate the present reservoir [10]

To achieve the best formation evaluation for the studied sequence, the petrophysical Archie's constants, such as the cementation exponent 'm', the tortuosity factor 'a' and formation water resistivity 'R_w' are needed to be determined. The Pickett's plot was used to determine the cementation exponent 'm' and the tortuosity factor 'a'. The cementation exponent increases southward from 1.6 in the north, to 2.14 in the south (Table 3), which indicates decreasing the petrophysical potentiality from the north to the south, from slightly cemented rocks to highly cemented rocks. We used the already published formation water resistivity 'R_w' values for each well corrected to the formation temperature [5,25]. The corrected 'R_w' values vary from 0.013 in the south to 0.023 ohm.m in the north (Belayim Marine field) (Table 3).

The mineral solver model using the modified Indonesian model was applied to the available well log data in a trial to detect the lithological composition and to characterize the petrophysical potentiality of the Matulla Formation including effective porosity, shale volume, oil and water saturation as well as net-pay thickness (Fig. 8). The validity of the modified Indonesian model could be attributed to the dispersed distribution of the clay. The mineralogical composition can be determined using the traditional crossplots, such as bulk density—neutron porosity, M–N and U_{maa} versus ρ_{maa}. Such crossplots indicate obvious shift toward the clastic facies (Fig. 8).

5 General Discussion

5.1 Depositional Environment and Mineralogical Composition

Based on the sequence stratigraphic concept [30,31] and the facies analyses, the Matulla Formation can be classified as a

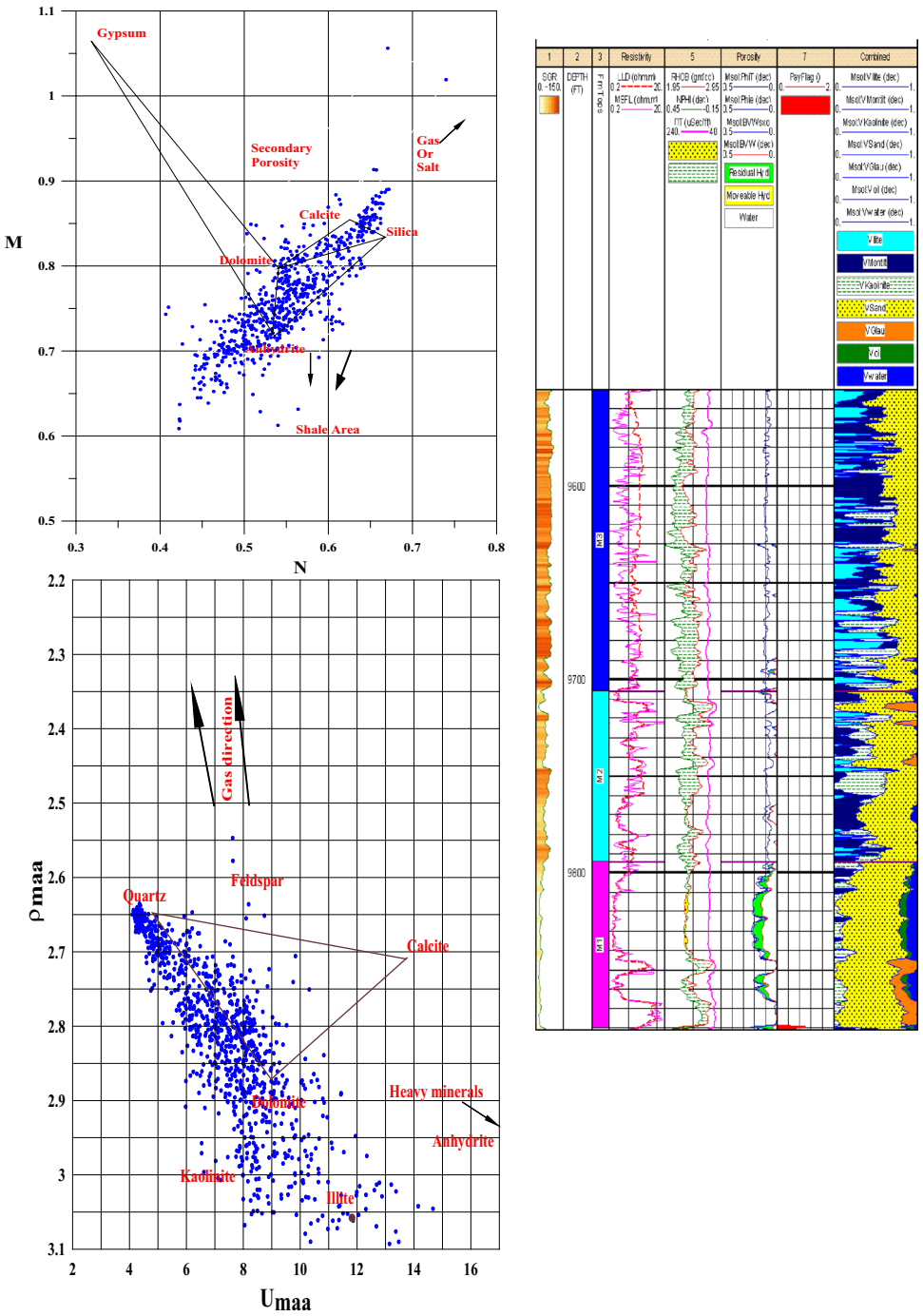

Fig. 8 Identification of the Matulla Formation lithology using traditional crossplots (after Schlumberger 1989) and mineral solver module using IP software in well A9 (Amal Field). Notice increases percentage of clays upward as response to progression of transgression. Umaa = apparent volumetric photoelectric absorption; ρmaa = apparent density of the matrix

second- order depositional sequence. This sequence consists of two systems tracts. Lowstand systems tract builds from a slope fan followed by a prograding complex. The crescent shape of logs, as well as the intercalations of sandstone and shale argued such interpretation (Fig. 3). The slope fan is interpreted to have been formed during the late relative fall and the early relative rise of the sea level, in which the thickest sands tend to occur in relatively narrow channels [31]. The slope fan is corresponding to the M1 unit. At the intermediate part of relative rise of sea level, the prograding complex sediments show a coarsening upward sequence. In the studied formation, the prograding complex corresponds to the M2 unit. An erosion surface separates the lowstand systems tract from the overlying transgressive systems tract (TST) (Fig. 3). The TST is interpreted to occur during the maximum rate of relative rise of sea level. In this systems tract, the sediments are mostly of mixed-layer illite/ montmorillonite clay content. The presence of some sandstone

Table 3 The values of petrophysical parameters of the Matulla Formation in the studied wells

Well	Formation water resistivity "R_w"	Cementation exponent "m"	Formation factor "a"
BM-85	0.023	1.6	0.62
A9	0.02	1.6	0.62
GS1	0.028	1.7	0.62
SB2	0.014	1.88	0.62
GS2	0.013	1.6	0.62
Sdk7	0.02	1.78	0.62
EZ	0.014	1.94	1
H-A4	0.017	2.14	1

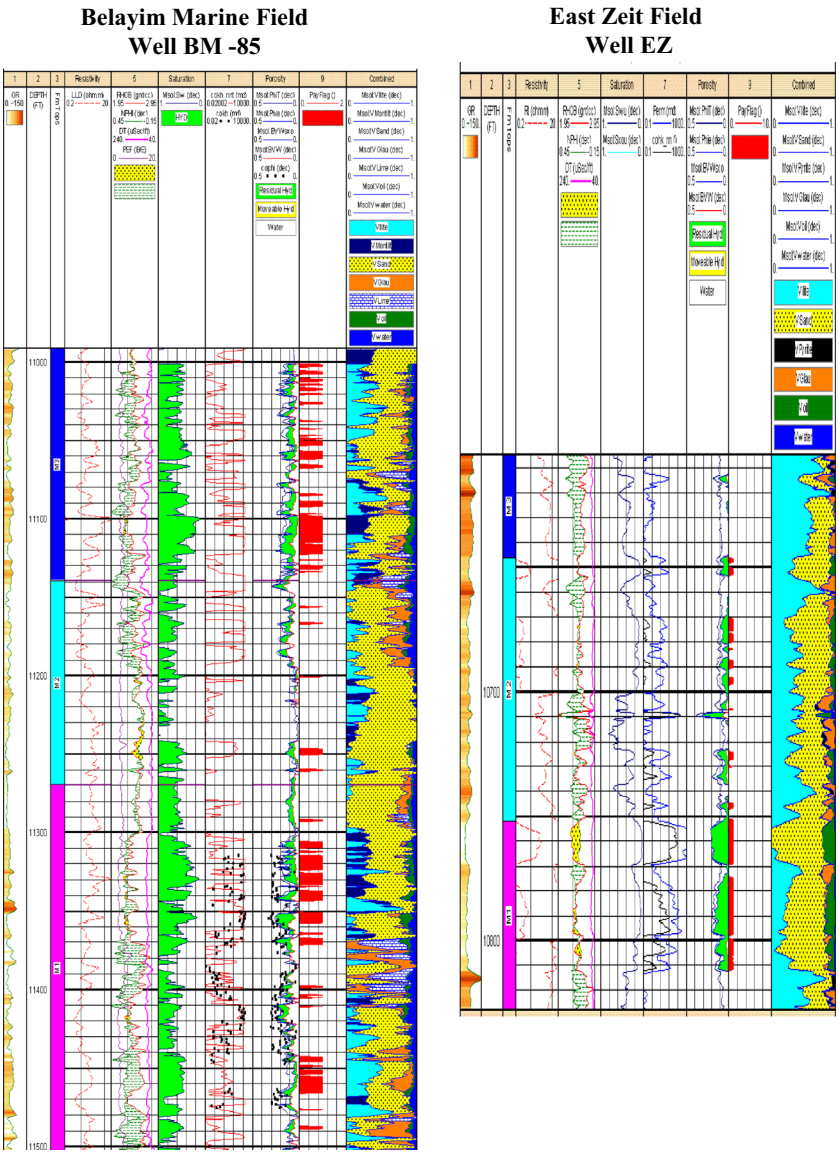

Fig. 9 Lithosaturation crossplots for BM-85 and EZ wells in the Central and Southern Gulf of Suez. Good matching was observed between measured and predicted permeability using the neural network as showed in BM-85 well. The model was applied for other wells as shown in EZ well

layers may be due to the reworking of the underlying prograding complex sands by erosion. The TST represents the M3 unit.

Lithologically, the Matulla Formation is a clastic sequence composed of arenaceous sandstone (Fig. 9). The *X*–*Y* crossplots in Fig. 6 show more reliability of the $U_{maa}-\rho_{maa}$ crossplot in determination the Matulla Formation lithology. The shift of the plotted points toward the illite and kaolinite clay minerals is obvious. Other crossplots, such as bulk density versus neutron and M–N, have no ability to identify the

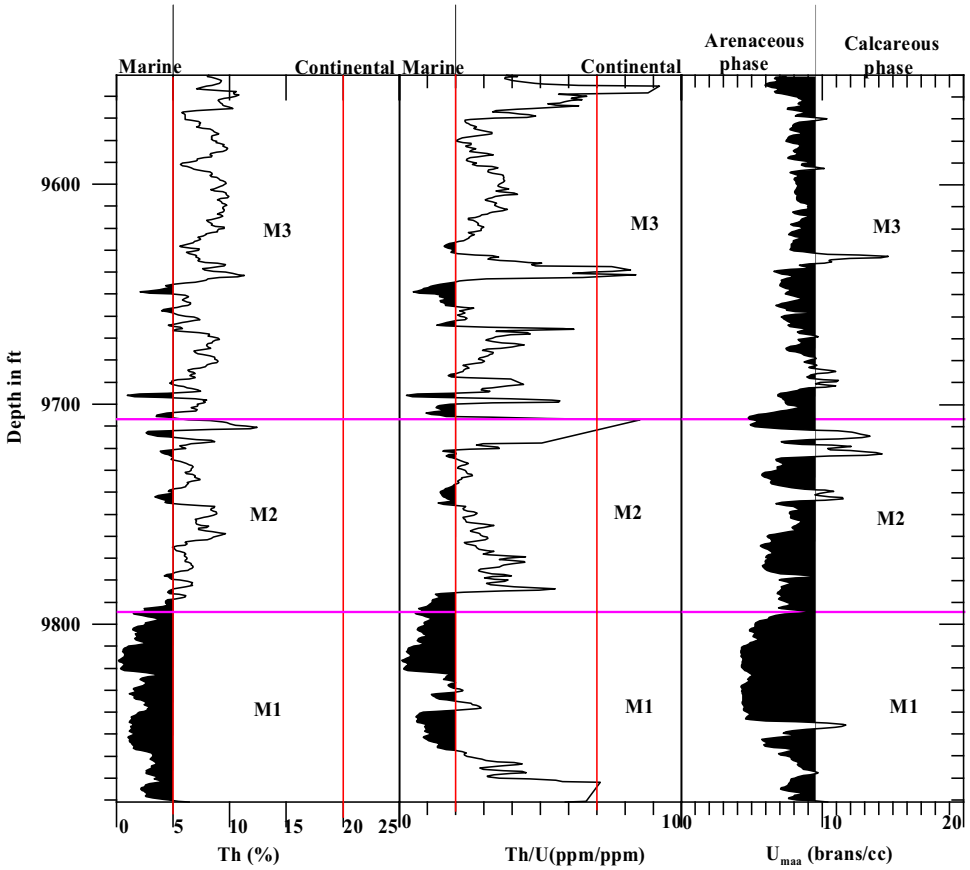

Fig. 10 The thorium concentration and thorium–uranium ratio against depth in well A9 (Amal Field), illustrating the possible environmental conditions that were prevailed during deposition of the Matulla Formation. Sudden change in uranium concentration argued an unconformity between M2 and M3 units. The Umaa against depth indicates that the Matulla sediments are mostly arenaceous with traces of calcareous sediments

accurate lithology due to the complicated lithology nature of the Matulla Formation.

Plotting the 'Th/U' ratio versus 'Th/K' ratio indicates that the upper unit (M3) of the studied Matulla Formation was deposited in mainly shallow marine condition of mainly mixed-layer clays (Fig. 7). On the other hand, the lower unit (M1) was deposited in mainly marine environment (Fig. 7). The same conclusion can be inferred from the crossplots of thorium concentration against depth and Th/U ratio against depth (Fig. 10). Pure marine environment was prevailed during deposition of the lower unit, as indicated from the former crossplot. However, the basal part of the lower unit indicates transitional conditions, as indicated from the later crossplot. This may be attributed to the presence of shaly to calcareous facies. Sudden change in Th/U ratio argued the presence of unconformity between upper and middle units.

The lithosaturation crossplots supported the conclusion that the studied facies consist mainly of quartz and various clay minerals. While traces of carbonaceous facies can be encountered in the northern part of the study area; glauconite and pyrite content tend to increase in the southern area. The presence of glauconite is considered as a diagnostic mineral indicator for the continental shelf quiet marine depositional environments. It has a tangible effect on the well logs causing a considerable increase in gamma ray, neutron and bulk density. On the other hand, an effective decrease in the formation resistivity was caused. Such effects can be significant with glauconite concentration above 8 % (Fig. 11).

5.2 Formation Evaluation and Reservoir Zonation

5.2.1 Formation Evaluation and Reservoir Characterization

Petrophysically and based on the lithological composition, the studied Matulla samples can be clustered into four lithological and petrophysical facies; namely, they are (1) sandstone, (2) argillaceous sandstone, (3) ferruginous sandstone and (4) limestone.

Prior to the formation evaluation, some *X*–*Y* plots have been presented to check the quality of the lithological facies of the Matulla reservoir. These *X*–*Y* plots are of great importance in order to test the quality of the measured petrophysical data and to test the interrelationship between the different petrophysical parameters. Hence, a model, which enables a calculation of different parameters, can be introduced.

The pore network volume of a given rock (expressed by porosity 'Ø') and its mineralogical composition expressed by its grain density are the main contributor to the bulk density 'ρ_b'. So plotting the bulk density against porosity for the

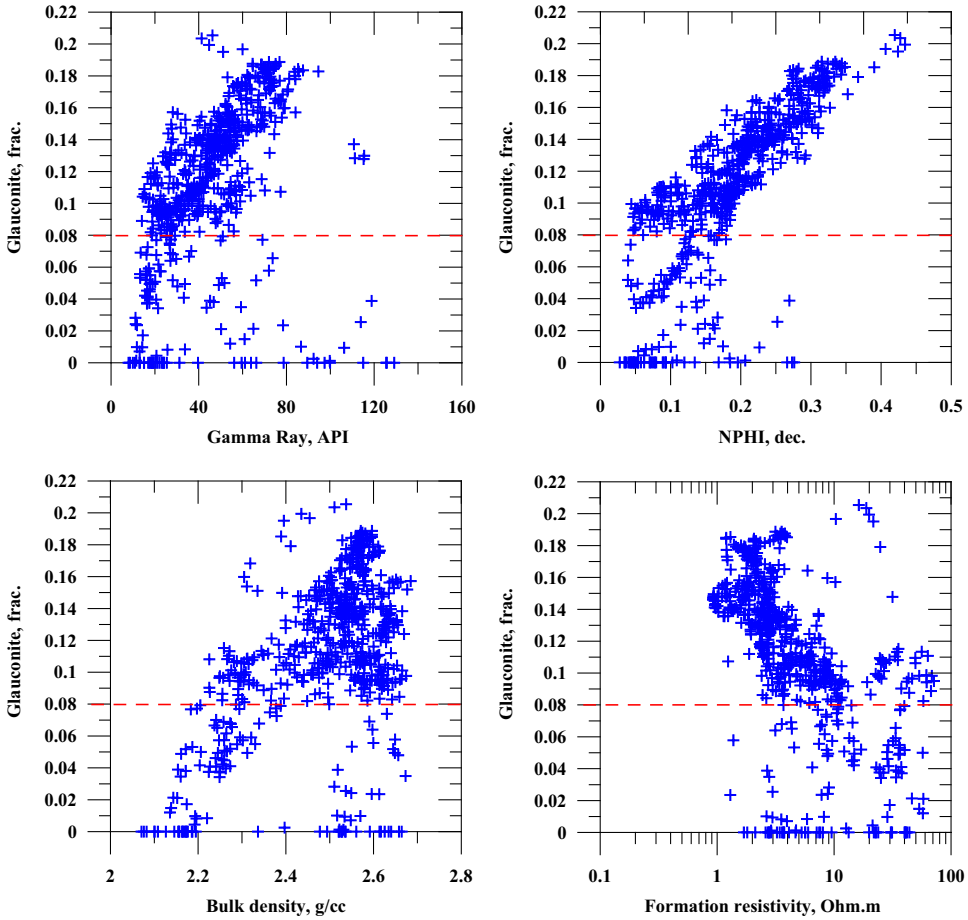

Fig. 11 Effect of glauconite concentration on the well log response as detected in well GS2 (GS373 Field). The effect was notably on gamma ray, density, neutron and resistivity logs. As noted, the considerable effect appears above 8 % glauconite

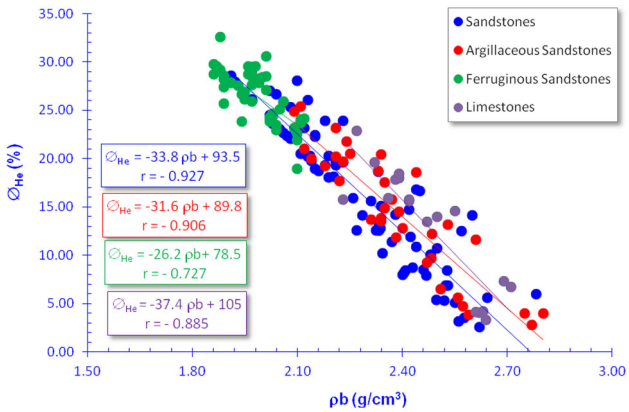

Fig. 12 Plotting the bulk density (ρ_b) versus the Helium porosity (Ø_{He}) as a QC procedure for testing the valid core data for the Matulla Formation in Belayim Marine and Hilal fields in the Gulf of Suez, Egypt

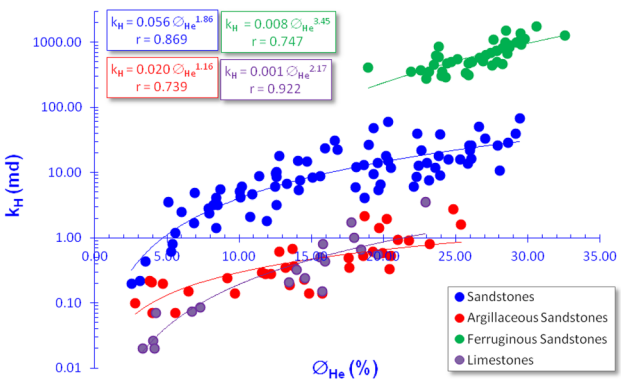

Fig. 13 Plotting horizontal core permeability ''k_H'' versus the measured helium porosity 'Ø_{He}' for the Matulla core samples in BM-85 and H-A4 wells, Gulf of Suez, Egypt

studied samples can be considered as a tool for quality control on the obtained data.

The bulk density values are mostly dependent on porosity with highly reliable interrelationships ($r \geq -0.727$, Fig. 12). The relatively low correlation coefficient 'r' encountered for the '$\text{Ø}_{He} - \rho_b$' relationship indicates some dependence of the bulk density on the grain density, which are highly scattered due to the heterogeneity of the mineralogical composition of the Matulla Formation. Scattering of grain density was matched particularly for the limestone facies ($2.71 \leq \rho_g \leq 3.47$ g/cm^3) and for some samples of the ferruginous sandstones due to high pyrite concentration.

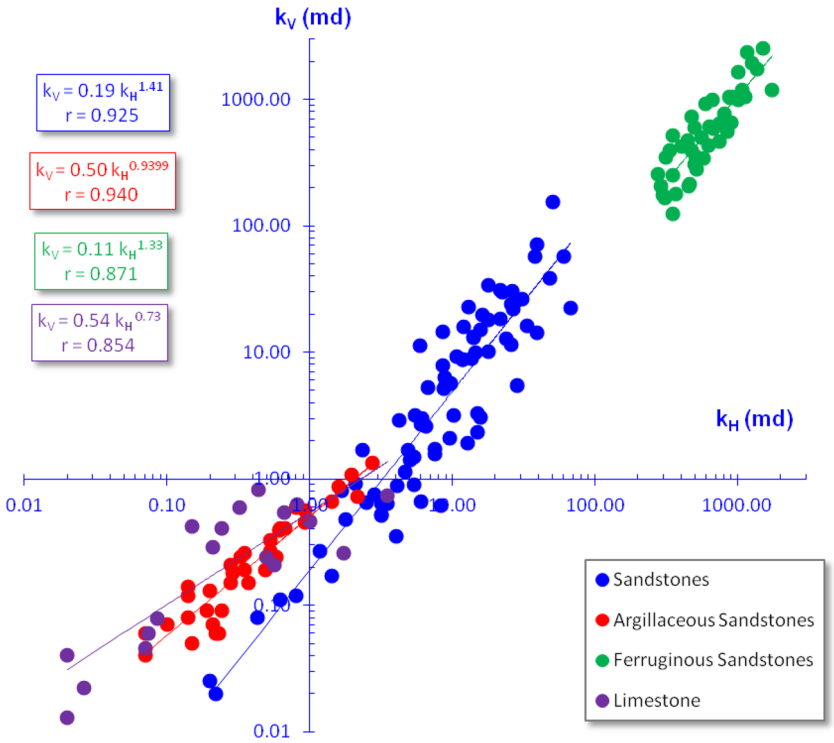

Fig. 14 Plotting the vertical and horizontal permeability measured for the valid core data as a tool for testing flow anisotropism in the Matulla Formation, Gulf of Suez Egypt

The porosity data of the present samples can be calculated in terms of the bulk density using the following equations.

Sandstones facies:	$Ø_{He} = 93.5 - 33.8\rho_b \quad (r = -0.927)$
Argillaceous sandstones facies:	$Ø_{He} = 89.8 - 31.6\rho_b \quad (r = -0.906)$
Ferruginous sandstones facies:	$Ø_{He} = 78.5 - 26.2\rho_b \quad (r = -0.727)$
Limestones facies:	$Ø_{He} = 105 - 37.4\rho_b \quad (r = -0.885)$

The statistical constant and multiplication factor of the obtained $Ø_{He}$–σ_b relationship are directly proportional to each other with the lowest values encountered for the ferruginous sandstone and the highest ones encountered for the limestone.

Based on the previous study carried out by Nabawy and Al-Azazi [10], it is declared that plotting the fluid summation porosity '$Ø_F$' versus the different petrophysical parameters is more scattered than plotting the helium porosity '$Ø_{He}$'. So, for the present study, it was recommended to use the '$Ø_{He}$' rather than the '$Ø_F$' values for further data processing. This recommendation was declared by obtaining less reliable plots for '$Ø_F$' versus the different petrophysical data of the studied Matulla Formation.

The greatly reduced permeability of the argillaceous facies should be attributed to some clay content, which may be of authigenic dispersed distribution, while that for the limestone facies may be attributed to the complexity of the pore throats or the vuggy nature of these pore spaces.

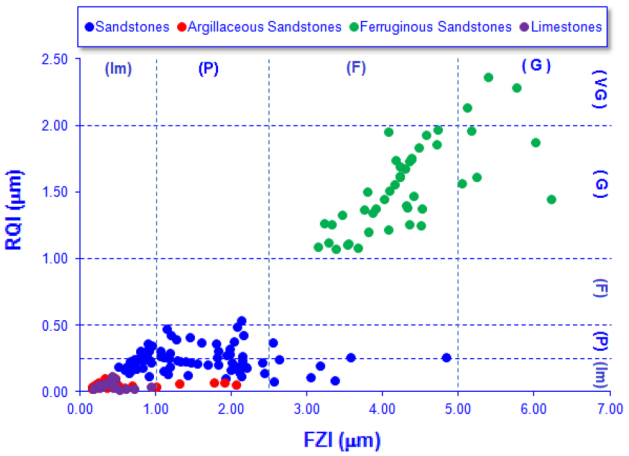

Fig. 15 Plotting the Reservoir Quality Index 'RQI' versus the flow zone indicator (FZI) for the Matulla Formation, Gulf of Suez, Egypt (ranks are shown in Table 2)

Increasing the vertical permeability more than the horizontal one cannot be attributed to depositional conditions. It is mostly attributed to the presence of a prevailed vertical fracturing system, which enhances the vertical permeability. As recommended by Nabawy and Al-Azazi [10], plotting permeability versus porosity should be restricted to plotting the horizontal permeability rather than the vertical one. However, using the vertical permeability is recommended rather than the horizontal one in case of the impervious rocks. Such rocks have no primary pore net volume but enhanced later by a fracturing system, which led to create a sensible fracture

pore volume, as observed in the fractured basement carbonate.

Permeability values 'k_H' for the different samples were plotted against the helium '$Ø_{He}$' as shown in Fig. 13. They are mostly exponentially dependent on porosity with relatively lower reliable relationship assigned for the ferruginous and the argillaceous sandstones.

The calculated empirical equations for the '$k_H - Ø$' relationships can be expressed as follows:

$$\text{Sandstone:} \quad k_H = 0.056Ø_{He}^{1.86} \quad (r = 0.869)$$

$$\text{Argillaceous sandstone:} \quad k_H = 0.020)Ø_{He}^{1.16} \quad (r = 0.739)$$

$$\text{Ferruginous sandstone:} \quad k_H = 0.008)Ø_{He}^{3.45} \quad (r = 0.747)$$

$$\text{Limestone:} \quad k_H = 0.001Ø_{He}^{2.17} \quad (r = 0.922)$$

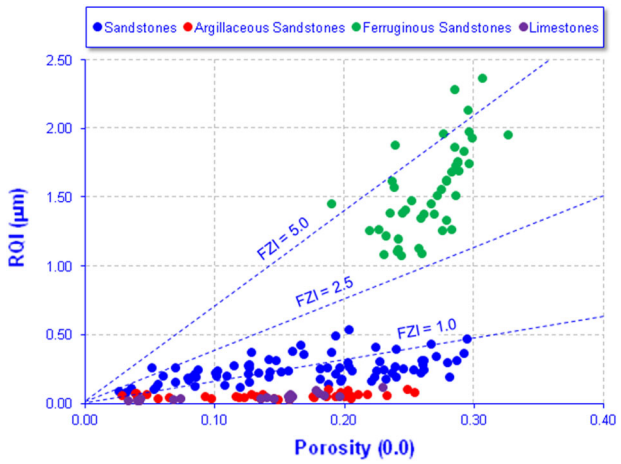

Fig. 16 Plotting the Reservoir Quality Index 'RQI' versus porosity for the Matulla Formation in the Gulf of Suez Egypt

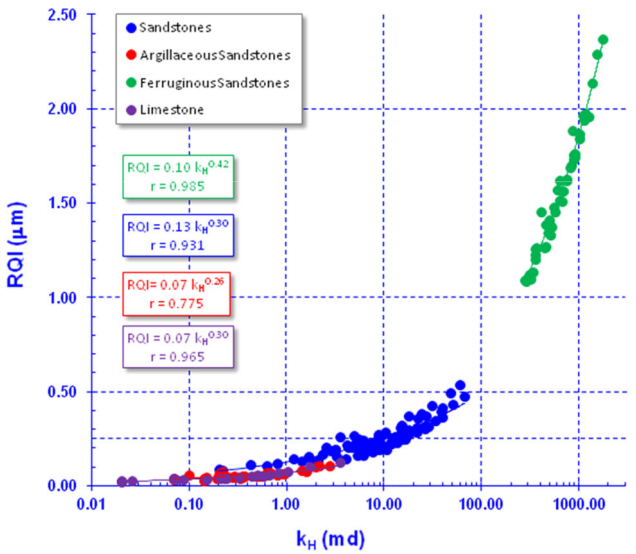

Fig. 17 Plotting the Reservoir Quality Index 'RQI' versus the horizontal permeability (K_H) for the Matulla Formation, Gulf of Suez Egypt

On the other hand, plotting the vertical permeability versus the horizontal one (Fig. 14) is a tool, which can be applied to examine the distribution of the hydraulic pore network of the studied formation in the 3D and its homogeneity/heterogeneity. A set of empirical equations is introduced to enable calculating the vertical permeability in terms of the horizontal one and vice versa as follows.

$$\text{Sandstone:} \quad k_V = 0.19k_H^{1.41} \quad (r = 0.925)$$

$$\text{Argillaceous sandstone:} \quad k_V = 0.50k_H^{0.94} \quad (r = 0.940)$$

$$\text{Ferruginous sandstone:} \quad k_V = 0.11k_H^{1.33} \quad (r = 0.871)$$

$$\text{Limestone:} \quad k_V = 0.54k_H^{0.73} \quad (r = 0.730)$$

As shown in Fig. 14, a very good interrelationship has been encountered between the horizontal and vertical permeability. The former equations show a multiplication factor, which increases mostly with the decrease in the exponent of k_H. This factor approaches 0.5 for both the argillaceous sandstone and the limestone with the exponent less than unity. These two facies showed permeability values in the rank of the impervious rocks. On the other side, permeability of the sandstone and the ferruginous sandstone facies is ranked as fair to very good with relatively lower multiplication factor 'intercept' up to 0.19 and higher exponent 'slope' up to 1.41. The intercept and slope of these two facies indicate that vertical permeability is mostly higher than the horizontal one (Fig. 14), e.g., higher fluid conductivity in the vertical direction due to the presence of fracture system.

The flow zone indicator 'FZI' is calculated as a function of the Reservoir Quality Index 'RQI'. The Reservoir Quality Index 'RQI' and the flow zone indicator 'FZI' for the studied facies were calculated using the normalized porosity index 'NPI' following Amaefule et al. [7] as follows.

$$\text{FZI} = \frac{\text{RQI}}{\text{NPI}} = \frac{0.0314\sqrt{k}/Ø}{Ø/(1-Ø)}$$

where k is permeability in md, and Ø is porosity, in volume fraction.

Taking into consideration the 'FZI' as well as water and oil saturation, the oil potentiality can be evaluated. In addition to characterizing the reservoir into flow zone units, the 'FZI' can be used to conduct a well-to-well correlation and to correlate horizontally any reservoir property or any well log data. The studied reservoir can be discriminated into impervious, poor, fair, good, very good and excellent reservoir of ranks 0–5, respectively (Table 2). Reservoir zonation can be conducted by measuring thickness of consequent beds having the same reservoir rank together in one flow unit.

Plotting the 'RQI' versus the 'FZI' (Fig. 15) indicates a good to very good reservoir quality and fair to good flow zone indicator for the ferruginous sandstone of the Matulla Forma-

tion. The sandstone facies is characterized by relatively lower reservoir ranks as impervious to poor 'RQI' and impervious to fair 'FZI'. The studied argillaceous sandstone facies as well as the limestone facies are characterized by impervious to poor 'FZI' rank and impervious 'RQI' rank.

Plotting the 'RQI' versus porosity as shown in Fig. 16 indicates that except for the ferruginous sandstones (good to very good 'RQI'), the studied facies are characterized by impervious to poor reservoir quality (RQI $\leq 0.5 \geq 2.5$). Moreover, the plotted parameters indicate that the 'RQI' of the sandstone and argillaceous sandstone is not dependent on their porosity values ($r \leq 0.51$), whereas the RQI is dependent on porosity for the ferruginous sandstone and limestone facies with relatively good reliability ($0.76 \leq r \leq 0.79$). This can be attributed to the complexity of pore spaces that have relatively low 'RQI' and fair to good permeability values. This means that the permeability rather than porosity is the main controlling factor for both RQI and FZI [10].

Plotting the 'RQI' versus the permeability values indicates a main dependence of the 'RQI' on permeability with very good to excellent reliability ($0.88 \leq r \leq 0.998$) (Fig. 17). The high reliability of the 'RQI–k_H' relationship introduces the permeability as a sensitive parameter, which can be used in reservoir zonation as an alternative for the 'RQI' and 'FZI'. The 'RQI' can be calculated in terms of the core permeability 'k_H' of the Matulla Formation in a very high reliability using the following empirical equations.

Sandstone:	$\mathrm{RQI} = 0.13k_H^{0.30}$ $(r = 0.931)$
Argillaceous sandstone:	$\mathrm{RQI} = 0.07k_H^{0.26}$ $(r = 0.775)$
Ferruginous sandstone	$\mathrm{RQI} = 0.10k_H^{0.42}$ $(r = 0.985)$
Limestone:	$\mathrm{RQI} = 0.07k_H^{0.30}$ $(r = 0.965)$

The multiplication factor fluctuates around 0.1 as the permeability exponent varies between 0.26 and 0.42, with very high reliability. The permeability exponent seems to be

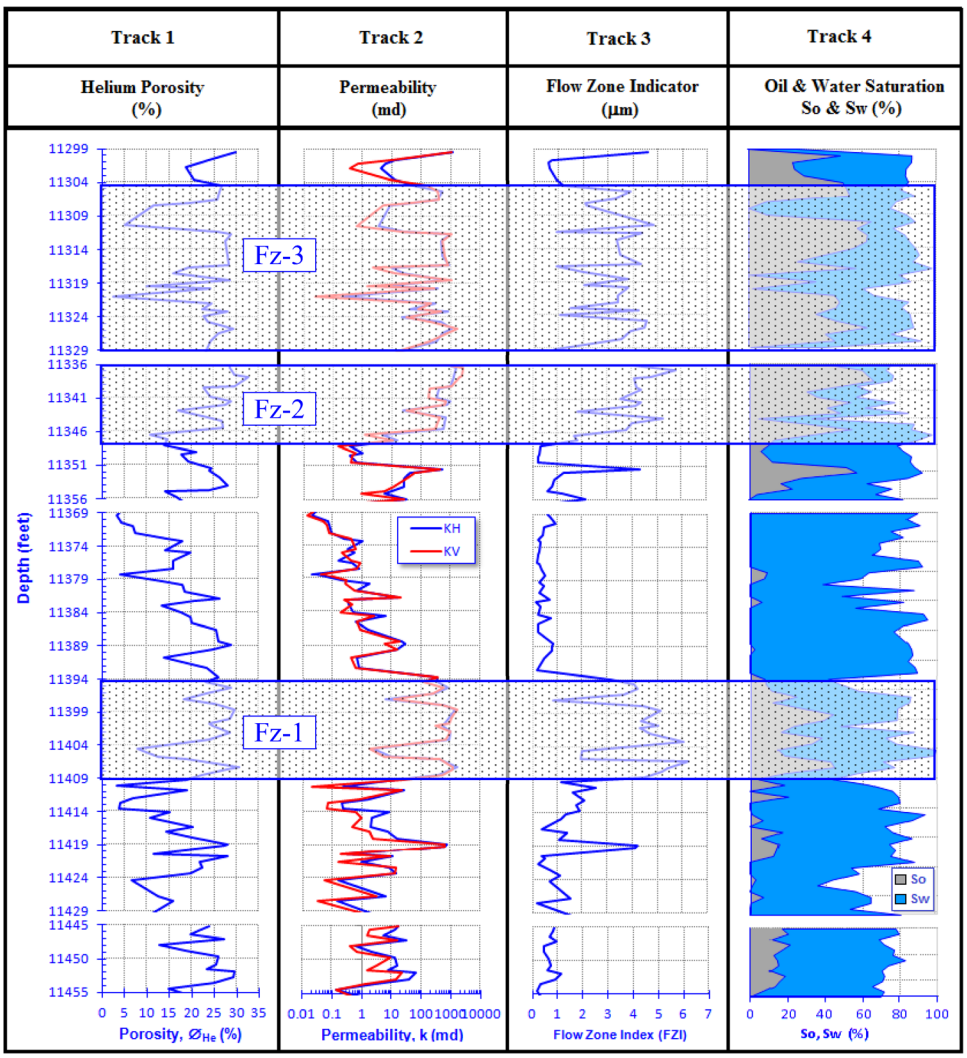

Fig. 18 Vertical matching of porosity, permeability, and flow zone indicator 'FZI' as well as both the water and hydrocarbon saturations versus depth for the Matulla Formation in BM-85 well (Belayim Marine oil field) to the north of the studied area in the Gulf of Suez, Egypt

related the 'FZI' ranks, where the ferruginous sandstone has the highest exponent and also the highest 'FZI', whereas the sandstone has relatively high FZI and permeability exponent (Figs. 15, 17).

5.2.2 Reservoir Zonation into Flow Units

Reservoir zonation is a statistical process, which can be applied to given reservoir characterizing it into flow zone units based on its measured porosity and permeability. Discriminating the reservoir into flow units, and assigning their values to all of pertinent physical properties give a better explanation for the reservoir heterogeneity and may be the base of well-to-well correlation. For the present study and following the recommendation of Nabawy and Al-Azazi [10], the helium porosity '$Ø_{He}$' and the horizontal permeability 'k_H' values were used for evaluation and zonation of the present Matulla reservoir into flow units. Reservoir zonation into flow units is based mostly on the flow zone indicator values 'FZI'.

In the following paragraphs, we aim to introduce the core analysis, as a tool used for the vertical reservoir zonation in parallel with the available well log data. So, the reservoir zonation will be conducted in two consecutive and comparable steps. The first preliminary step will be restricted to the cored sequences using the core analysis, and the second is more general through the logged parts in the Matulla Formation based on the well log data.

Taking the water and oil saturation into consideration, the reservoir zonation is carried out based on porosity, permeability and 'FZI'. Cutoff values will be taken following the proposed classification in Table 2, where the permeability cutoff equals to 1 md, porosity as 5 % and FZI cutoff equals to 1, which are equivalent to the poor reservoir rank. Consequently, three flow units 'FU' can be declared from the available BM-85 well (Belayim Marine oil field) core data

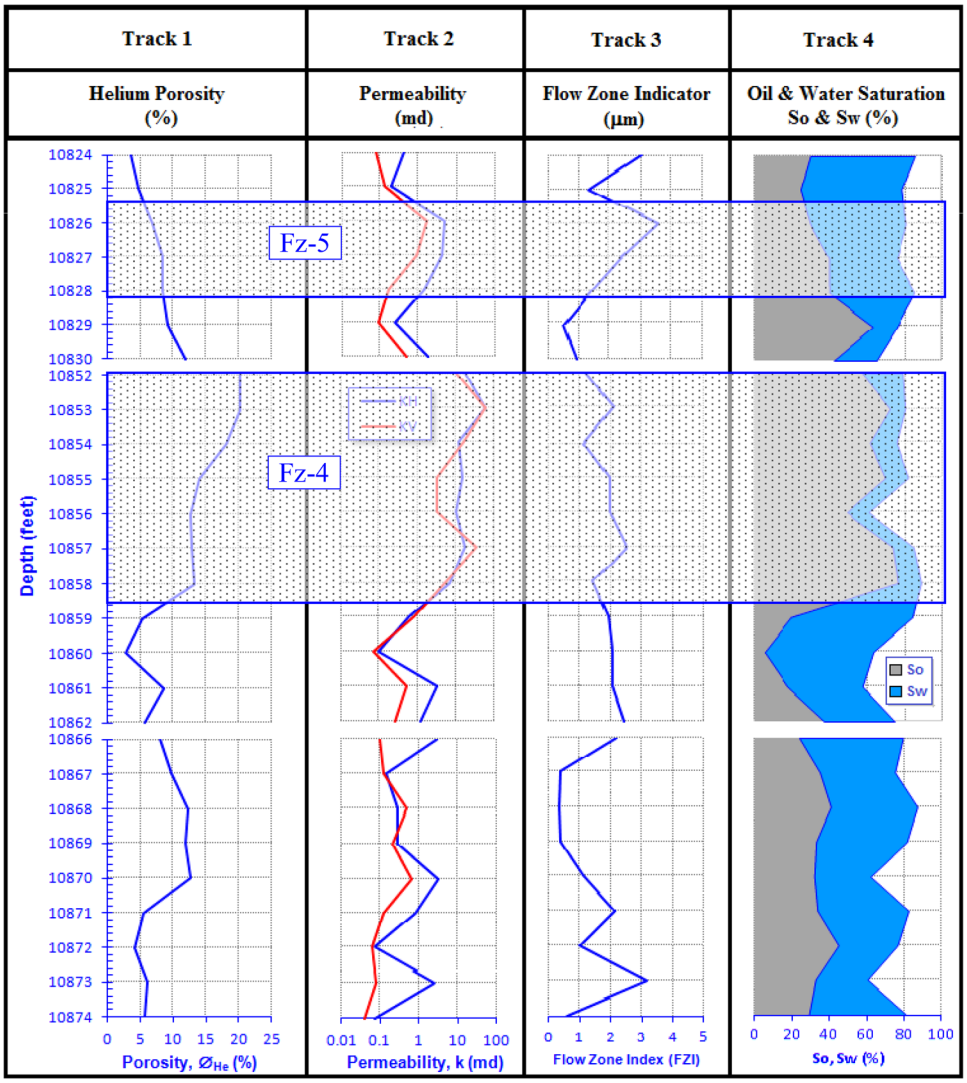

Fig. 19 Vertical matching of porosity, permeability and flow zone indicator 'FZI' as well as both the water and hydrocarbon saturations versus depth for the Matulla Formation in H-A4 well (Hilal oil field) to the south of the study area in the Gulf of Suez, Egypt

(Fig. 18). The lower depositional unit 'M1' that declared from the well log data can be further subdivided based on the core data into three flow units. The upper unit 'FU-3' extends from depth 11304.5 down to 11329 ft (thickness 24.5 ft) with poor to good permeability and poor to very good porosity but ranked as poor to fair flow zone unit ($1 \leq \text{FZI} \leq 5$). The second flow unit 'FU-2' with a less thickness (11 ft) is characterized by poor to good porosity and permeability and ranked as poor to fair flow unit. 'FU-1' is characterized by poor to good permeability and poor to very good porosity but ranked relatively higher than the other two flow units; it is ranked also as poor to good flow unit. The ranked flow units have less than 50 % water saturation and indicate heterogeneity of the flow properties of the Matulla Formation with many shale streaks and intercalations having bad 'negligible' reservoir properties. The water saturation indicates presence of more than one water bodies and oil–water contact, e.g., at depths 11,369 and 11,410 ft, while the oil saturation may indicate presence of some oil shows above the cored intervals at depth <11,299 in BM-85 well (Fig. 18).

To the south of the studied area in Hilal field in well H-A4, the cored interval is thin (24 ft thick). Two thin flow units can be traced; the first one (3 ft) extends from depth 10825.5 to 10828.5 ft, and the other one is 6.5 ft. The upper flow unit (FU-5) is characterized by poor porosity and permeability but ranked as poor to fair flow unit (Fig. 19). The lower unit 'FU-4' has better reservoir properties with good to very good porosity, poor to fair permeability and poor flow unit properties ($1 \leq \text{FZI} \leq 2.5$). The water and oil saturations indicate good oil shows in the lower part of well H-A4, but with negligible to poor porosity and negligible to poor permeability, i.e., ranked as impervious to poor flow units. The net-pay zone in well H-A4 (Hilal field) to the south is 9.5 ft, whereas to the north in BM-85, it is 50.5 ft with better reservoir quality indicating enhancement of reservoir quality properties of the Matulla Formation to the north of the studied area in the central Gulf of Suez.

The thin and relatively low reservoir properties of the middle and upper parts of the Matulla Formation to the south of the studied area may be attributed to shallower and restricted depositional conditions, which led to formation of glauconite, which in turn caused more complexity of the pore spaces and reduction in the permeability and the reservoir quality.

Table 4 Pay cutoff results in the studied wells

Field	Zone	Gross	Net	Net/gross	Φ_{avg}	S_{wavg}	V_{shavg}	PhiH	PhiSoH	VshH
Belayim Marine (BM-85)	M3	147.5	47.5	0.32	0.163	0.34	0.32	7.74	5.07	15.16
	M2	130	10	0.08	0.139	0.44	0.17	1.4	0.78	1.74
	M1	233	56	0.24	0.179	0.37	0.25	10	6.34	14.36
Amal (A9)	M3	155	–	–	–	–	–	–	–	-
	M2	88	–	–	–	–	–	–	–	–
	M1	87	1.25	0.016	0.187	0.22	0.07	0.23	0.18	0.09
GS365 (GS1)	M3	70	7	0.1	0.264	0.43	0.17	1.85	1.04	1.18
	M2	96	21.5	0.24	0.215	0.36	0.15	4.6	2.96	3.28
	M1	72	17	0.23	0.149	0.42	0.12	2.5	1.47	2.1
SB374 (SB2)	M3	64.5	–	–	–	–	–	–	–	–
	M2	162	71.5	0.44	0.15	0.24	0.2	10.7	8.13	14.3
	M1	87.5	11.75	0.134	0.121	0.31	0.25	1.42	0.97	3
GS373 (GS2)	M3	192	6.25	0.03	0.21	0.29	0.137	1.31	0.93	0.86
	M2	83	32	0.39	0.18	0.35	0.08	5.82	3.8	2.63
	M1	163	57.5	0.35	0.189	0.37	0.09	10.88	6.89	5.17
Sidki (Sdk7)	M3	79	14.5	0.18	0.215	0.26	0.18	3.12	3.23	2.7
	M2	181.5	64	0.35	0.188	0.27	0.2	12.05	8.8	12.7
	M1	120.5	51	0.42	0.179	0.31	0.19	9.11	6.3	9.7
East Zeit (Ez)	M3	41	–	–	–	–	–	–	–	–
	M2	106	27.75	0.26	0.133	0.14	0.29	3.68	3.15	7.97
	M1	76	51.75	0.68	0.172	0.09	0.17	8.88	8.1	8.78
Hilal (H-A4)	M3	78	1	0.013	0.113	0.34	0.28	0.11	0.07	0.28
	M2	91	54.25	0.59	0.141	0.28	0.17	7.67	5.5	9
	M1	109	72.25	0.66	0.153	0.4	0.13	11.1	6.67	9.6

PhiH = PHI*net; PhiSoH = (1-sw)*phi*net; VshH = Vsh* net

Finally and after checking the quality of the studied data and modeling the petrophysical parameters, the net-pay thickness has been calculated based on 10 % porosity, 35 % clay content and 50 % water saturation as cutoff values. The net-pay thickness of Matulla Formation in the studied southern central Gulf of Suez varies from 1 to about 129 ft with an average value of 85 ft (Table 4). The net-to-gross thickness ratio is ranged from 0 to 43 % with an average value of 25 %. It can be observed that the net-to-gross thickness shows general increasing trend from M3 to M1, as shown in wells H-A4 and GS373-2. The net-pay thickness in M3 reached zero in several wells such as EZ and SB. Generally, it can be concluded that the main productive zones are M1 as well as M2 units of Matulla Formation within the rock types RT1, RT2, RT3 and RT4, which are mostly composed of sandstones and glauconitic sandstones.

6 Conclusions

Application of the Indonesian mineral solver model to the available well log data for the Matulla formation of some selected wells in the Gulf of Suez indicates that the Matulla Formation is composed mainly of intercalations of sandstones and pelagic sediments. It can be subdivided into three depositional units M1 to M3 (corresponding to second-order depositional sequence). The Matulla sequence consists of two systems tracts. The lower lowstand systems tract consists of slope fan (M1), followed by prograding complex (M2). Above them, a transgressive systems tract was developed (M3), with a distinct unconformity surface separating the middle unit from the upper one.

The sandstone ratio decreased upward, as a response to the rise in sea level. Restrictive depositional conditions prevailed southward, which allowed the glauconitization process to take place as a consequence of diagenetic alteration of some sedimentary deposits. The effect of glauconite is obvious on the well logs above 8 % of glauconite concentration. At this percentage, it causes a significant decrease in the resistivity, as well as increase in gamma ray, density and neutron logs. However, the petrophysical model, using the IP program, has the ability to overcome such problems.

Seven rock types can be identified within the Matulla sediments. These types are sandstone, fine-grained glauconitic sandstone, shaly-glauconitic sandstone, argillaceous sandstone, ferruginous sandstone, and argillaceous sandstone with mixed-layer clays. Good reservoir quality is representative of the first two rock types and nonreservoir quality the last three rock units.

The petrophysical reservoir evaluation via determination of effective porosity, shale content, water saturation and net-pay thickness indicates that the Matulla Formation can be considered as a good-quality reservoir in the lower and middle units. The studied core data supported the processed well log data through the petrophysical facies discrimination and reservoir zonation. Four petrophysical and lithological facies can be identified; namely, they are sandstones, argillaceous sandstones, ferruginous sandstones and limestones. The ferruginous sandstones seem to have the best reservoir properties in Matulla Formation ($Ø_{av}$ = 26.3 %, k_{Hav} = 722md, Sw_{av} = 35.7 %, So_{av} = 35.9 %, and FZI_{av} = 4.28). Based on the flow unit concept and reservoir zonation, the lower unit (M1) of Matulla formation can be subdivided into three flow units (FU 1–3), whereas other two flow units (FU 4 and 5) are referred to the middle and upper units (M2 and M3) of Matulla Formation.

Acknowledgments The authors would like to acknowledge The Egyptian General Petroleum Corporation 'E.G.P.C.', Gulf of Suez Company (GUPCO) and Belayim Petroleum Company (Petrobel) for releasing the well log and core analysis data and the license for data processing and interpretation.

References

1. Patton, T.L.; Moustafa, A.R.; Nelson, R.A.; Abdine, S.A.: Tectonic evolution and structural setting of the Suez rift. In: Landon, S.M. (ed.) Interior Rift Basins, pp. 9–55. AAPG Memoir 59 (1994)
2. Steen, G.; Helmy, H.: Pre-Miocene evolution of the Gulf of Suez region. Gulf of Suez Petroleum Company, unpublished report, no. ER 82-1 (1982)
3. Hasouba, M.; Abd El Shafy, A.; Mohamed, A.: Nezzazat Group—reservoir geometry and rock types in the October field area, Gulf of Suez. In: 11th EGPC Petroleum Exploration and Production Conference 1, pp. 293–317 (1992)
4. Marttila, R.K.; El Bahr, M.: Evaluation of a lithology complex reservoir (Nezzazat Group) in the Gulf of Suez. In: 12th EGPC Exploration and Production Conference 2, pp. 472–482 (1994)
5. El Bahr, M.; Patchett, J.G.; Wiley, R.: Modeling the effects of glauconite on some openhole logs from the Lower Senonian in Egypt. In: 11th EGPC Petroleum Exploration and Production Conference 1, pp. 494–514 (1992)
6. El-Azabi, M.H.; El-Araby, A.: Depositional framework and sequence stratigraphic aspects of the Coniacian–Santonian mixed siliciclastic/carbonate Matulla sediments in Nezzazat and Ekma blocks, Gulf of Suez, Egypt. Journal of African Earth Sciences **47**, 179–202 (2007)
7. Amaefule, J.O.; Altunbay, M.; Tiab, D.; Kersey, D.G.; Keelan, D.K.: Enhanced reservoir description: Using core and log data to identify hydraulic (flow) units and predict permeability in uncored intervals/wells. SPE 26436. Presented at the Annual Technical Conference and Exhibition, Houston, TX, 205-220 (1993)
8. Tiab, D.; Donaldson, E.C.: Petrophysics, Theory and practice of measuring reservoir rock and fluid transport properties, Gulf Publ. Co., Houston, Texas, pp. 205-220 (1996)
9. Al-Dhafeeri, A.M.; Nasr-El-Din, H.A.: Characteristics of high-permeability zones using core analysis, and production logging data. J. Petrol. Sci. Eng. **55**, 18–36 (2007)
10. Nabawy, B.S.; Al-Azazi, N.A.S.: Reservoir zonation and discrimination using the routine core analyses data: the Upper Jurassic Sab'atayn sandstones as a case study, Sab'atayn basin, Yemen. Arab. J. Geosci. doi:10.1007/s12517-014-1632-3 (2014)

11. Said, R.: Cretaceous paleogeographic maps. In: Said, R. (ed.) Geology of Egypt, pp. 439–449 (1990)
12. Kerdany, M.T.; Cherif, O.H.: Mesozoic. In: Said, R. (ed.) Geology of Egypt, pp. 407–438 (1990)
13. Moustafa, A.M.: Block faulting in the Gulf of Suez. In: Egyptian General Petroleum Corporation, 5th Exploration Seminar, 36 p. (1976)
14. Garfunkel, Z.; Bartov, Y.: The tectonics of the Suez rift. Geological Survey of Israel Bulletin 71, 45 p. (1977)
15. Montenat, C.; Ott d'Estevou, P.; Purser, B.: Tectonic and sedimentary evolution of the Gulf of Suez and the northwestern Red Sea: a review. In: Montenat, C. (ed.) Geological Studies of the Gulf of Suez, Northwestern Red Sea Coasts, Tectonic and Sedimentary Evolution of Neogene Rift, pp. 7–18. Documents et Travaux Institut Geologique Albert de Lapparent 10 (1986)
16. Richardson, M.; Arthur, M.A.: The Gulf of Suez-northern Red Sea Neogene rift: a quantitative basin analysis. Mar. Pet. Geol. **5**, 247–270 (1988)
17. Bosworth, W.; Crerello, P.; Winn Jr., R.D.; Steinmetz, J.: Structure, sedimentation, and basin dynamics during rifting of the Gulf of Suez. In: Purser B.H.; Bosence, D.W.J. (eds.) Sedimentation and Tectonics of Rift Basins: Red Sea—Gulf of Aden, pp. 78–96 (1998)
18. Bosworth, W.; McClay, K.: Structural and stratigraphic evolution of the Gulf of Suez rift, Egypt: a synthesis. In: Ziegler P.A.; Cavazza W.; Roberston A.H.F.; Crasquin-Soleau S. (eds.) Peri—Tethys Memoir 6: Peri – Tethyan Rift/ Wrench Basins and Passive Margins, pp. 567–606 (2001)
19. Winn, R.D. Jr.; Crevello, P.D.; Bosworth, W.: Lower Miocene Nukhul Formation, Gebel el Zeit, Egypt: Model for structural control on early synrift strata and reservoirs, Gulf of Suez. AAPG Bull. **75**, 1871–1890 (2001)
20. Younes, A.I.; McClay, K.: Development of accommodation zones in the Gulf of Suez—Red Sea rift, Egypt. AAPG Bull. **86**(6), 1003–1026 (2002)
21. Alsharhan, A.S.: Petroleum geology and potential hydrocarbon plays in the Gulf of Suez rift basin, Egypt. AAPG Bull. **87**(1), 143–180 (2003)
22. Omran, M.A.; El Sharawy, M.S.: Tectonic evolution of the Southern Gulf of Suez, Egypt: a comparison between depocenter and near peripheral basins. Arab. J. Geosci. **7**(1), 87–107 (2014)
23. Rowan, R.: Modern salt tectonics. In: Petroleum Technology Transfer Council Workshop, 26 July, Mississippi (2000)
24. Warren, J.K.: Evaporites: Sediments, Resources and Hydrocarbons. Springer, New York (2006)
25. Egyptian General Petroleum Corporation, EGPC: Gulf of Suez oil fields (a comprehensive overview) (1996)
26. El Sharawy, M.S.: Geology and tectonic of Younis and Nessim oilfields, Gulf of Suez, Egypt. M.Sc., Mansoura University, 211 p. (2001)
27. Adams, J.A.S.; Weaver, C.E.: Thorium to uranium ratios as indicators of sedimentary processes: example of concept of geochimical faciès. AAPG Bull. **42**, 387–430 (1958)
28. Ahmed, U.; Cary, S.F.; Coates, G.R.: Permeability estimation: the various sources and their interpretations. JPT, pp. 578–587 (1991)
29. Timur, A.: An investigation of permeability, porosity, and residual water saturation relationships for sandstone reservoirs. Log Anal. **9**, 8–17 (1968)
30. Neal, J.; Risch, D.; Vail, P.: Sequence stratigraphy—a global theory for local success. Oilfield Rev. **5**(1), 51–62 (1993)
31. Mitchum, R.M. Jr., Sangree, J.B., Vail, P.R., Wornardt, W.W.: Recognizing sequences and systems tracts from well logs, seismic data, and biostratigraphy: examples from the late Cenozoic. In: Weimer, P., Posamentier, H.W. (eds.) Siliciclastic Sequence Stratigraphy: Recent Developments and Applications. American Association of Petroleum Geologists, Memoir 58, pp. 163–197 (1993)